

Air quality, health and equity implications of electrifying heavy-duty vehicles

Received: 20 December 2022

Accepted: 21 August 2023

Published online: 5 September 2023

 Check for updates

Sara F. Camilleri¹✉, Anastasia Montgomery¹, Maxime A. Visa¹, Jordan L. Schnell^{1,2,6,7}, Zachariah E. Adelman³, Mark Janssen³, Emily A. Grubert⁴, Susan C. Anenberg⁵ & Daniel E. Horton^{1,2}

Heavy-duty vehicles (HDVs) disproportionately contribute to the creation of air pollutants and emission of greenhouse gases—with marginalized populations unequally burdened by the impacts of each. Shifting to non-emitting technologies, such as electric HDVs (eHDVs), is underway; however, the associated air quality and health implications have not been resolved at equity-relevant scales. Here we use a neighbourhood-scale (~1 km) air quality model to evaluate air pollution, public health and equity implications of a 30% transition of predominantly diesel HDVs to eHDVs over the region surrounding North America's largest freight hub, Chicago, IL. We find decreases in nitrogen dioxide (NO₂) and fine particulate matter (PM_{2.5}) concentrations but ozone (O₃) increases, particularly in urban settings. Over our simulation domain NO₂ and PM_{2.5} reductions translate to ~590 (95% confidence interval (CI) 150–900) and ~70 (95% CI 20–110) avoided premature deaths per year, respectively, while O₃ increases add ~50 (95% CI 30–110) deaths per year. The largest pollutant and health benefits simulated are within communities with higher proportions of Black and Hispanic/Latino residents, highlighting the potential for eHDVs to reduce disproportionate and unjust air pollution and associated air-pollution attributable health burdens within historically marginalized populations.

Electrifying the transportation sector is an ongoing and accelerating climate change mitigation action that will bring a range of co-benefits that could potentially reduce long-standing environmental injustices associated with air pollutant exposure^{1,2}. Despite representing only 6% of total on-road vehicles in the United States³, medium-to-heavy-duty trucks and buses are the second largest source of transportation CO₂ emissions (~27% (ref. 4)), the largest contributors to on-road NO_x (~32% (ref. 2))—an Environmental Protection Agency (EPA) criteria pollutant and key precursor in ozone (O₃) formation—and a substantial on-road source of particulate matter (PM)⁵. In the United States, traffic-related pollution contributes to yearly PM_{2.5}- and O₃-related premature deaths of

between 12,000 and 31,000 (ref. 6) and 43% of traffic-related PM_{2.5} and O₃ mortality has been linked to on-road diesel pollution⁷. Traffic-related air pollution has also been linked to paediatric asthma incidence⁸ and circulatory and ischaemic heart disease mortality⁹. Air pollution hotspots from heavy-duty vehicles (HDVs) typically occur in urban settings, areas close to interstate highways, and along truck routes^{10–12}, and with more than 45 million people living within 300 feet of major road networks in the United States¹³—the majority of whom are people of colour¹⁴—HDV-related emissions disproportionately impact minoritized populations^{15–19}.

Transitioning from traditional internal combustion HDVs to electric HDVs (eHDVs) is one commonly espoused climate mitigation

¹Department of Earth and Planetary Sciences, Northwestern University, Evanston, IL, USA. ²Trienens Institute for Sustainability and Energy, Northwestern University, Evanston, IL, USA. ³Lake Michigan Air Directors Consortium, Rosemont, IL, USA. ⁴Keough School of Global Affairs, University of Notre Dame, Notre Dame, IN, USA. ⁵Department of Environmental and Occupational Health, Milken School of Public Health, George Washington University, Washington, DC, USA. ⁶Present address: Cooperative Institute for Research in Environmental Sciences, University of Colorado, Boulder, CO, USA.

⁷Present address: NOAA/Global Systems Laboratory, Boulder, CO, USA. ✉e-mail: sara.camilleri@northwestern.edu

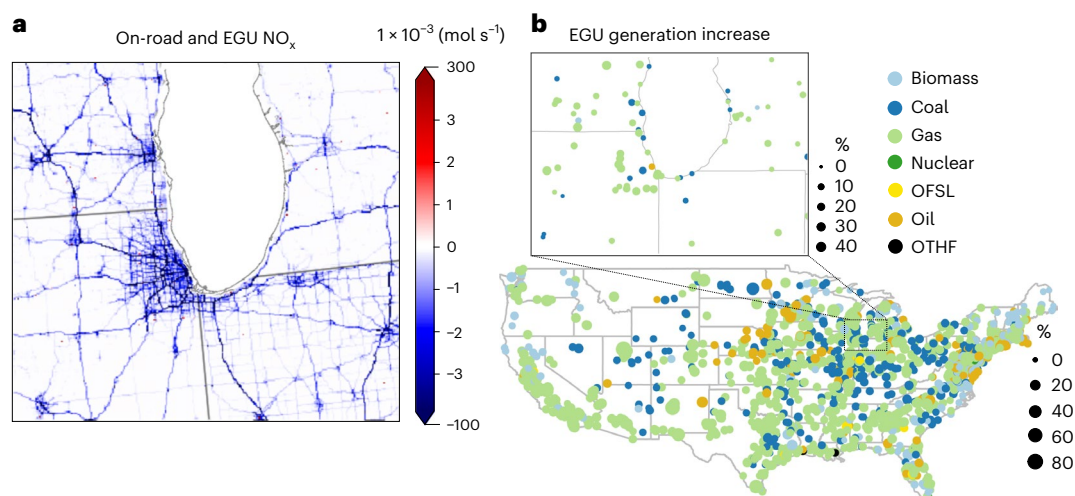


Fig. 1 | Emission changes. **a, b**, On-road and EGU NO_x emission changes compared with the baseline scenario in mol s⁻¹ (**a**) and EGU percentage generation increase by fuel type following 30% electrification of HDVs (**b**). Numbers at the tails of colour bar in **a** indicate minimum and maximum differences in emissions within the domain. Note that increases in emissions are depicted in **a**; however, they are restricted to grid cells that contain EGUs. While accounting for clean electricity

generation from emission-free renewable EGUs (other than nuclear), the increase in electricity demand depicted in **b** represents only the portion of electricity sourced from non-renewable powered EGUs and nuclear EGUs. OFSL and OTHF fuel types refer to other fossil fuel types and fuel derived from waste heat, unknown or purchased sources, respectively.

strategy³; however, the associated air-quality and public health implications of such a transition have not yet been widely assessed at the fine (-1 km) spatial resolutions needed to determine differential exposure between population subgroups in urban settings²⁰; a critical need for environmental justice objectives such as the US Federal Government's Justice40 Initiative²¹. While changes in GHG emissions brought about by eHDV adoption (for example, CO₂), can be directly related to global atmospheric abundances, determining overall changes in air pollutant concentrations is more challenging due to non-linear chemistry, the formation of secondary pollutants, the effects of dynamic meteorology, and other nuances associated with a region's chemical regime.

Estimating the air quality and health implications from emission changes can be done at high spatial resolutions using reduced-complexity models (RCMs²²)—tools that are ideal for testing a multitude of policies when computational resources are limited^{23,24}. However, the advantages of an RCM come at the expense of higher uncertainties²⁵, coarser temporal resolution, and the inability to assess changes in secondary pollutants such as O₃ (ref. 24)—a pollutant associated with adverse traffic-related health impacts. Chemical transport models (CTMs) on the other hand, are more computationally expensive but include the complex atmospheric chemistry and meteorological feedbacks necessary for representing changes in secondary pollutants while also allowing for simulations at short temporal scales, in line with regulatory air quality standards. General agreement on the potential of electric vehicles (EVs) to reduce GHGs as well as NO_x and PM_{2.5} concentrations exists among CTM studies^{26–31}; however, the spatial distribution of these differences at neighbourhood scales is not fully captured when coarse resolution CTMs are used^{29–31}. Unlike NO₂ and PM_{2.5}, evidence documenting O₃ changes that result from EV adoption is inconsistent, with national studies suggesting widespread O₃ reductions^{29,31} but finer-scale studies, of which only two are United States based, identifying isolated increases^{26–28,32}. Few CTM studies have estimated the air pollution-related health impacts due to EVs³⁰ particularly at equity-relevant scales²⁶, with no study thus far estimating the associated environmental justice implications of eHDV adoption.

In this Article, we use a regulatory-grade two-way coupled CTM framework (WRF-CMAQ) to characterize neighbourhood-scale (1.3 km) changes in primary and secondary pollutant concentrations (that is, NO₂, O₃ and PM_{2.5}) when a portion of the on-road HDV fleet is

instantaneously converted to eHDVs. We focus our analysis on the region surrounding North America's largest freight hub, Chicago, IL³³, and leverage the most recent census tract-level health data to estimate census tract-level variability in eHDV-driven health impacts that account for the underlying susceptibilities of exposed populations. Additionally, we assess equity outcomes by characterizing how eHDV adoption could alter air pollution and health impact disparities among racial/ethnic subgroups. Our approach accounts for on-road and refuelling infrastructure emission changes as well as altered emissions from electricity generation units (EGUs) due to eHDV battery charging demands.

Results

Changes in emissions

For most chemical species, an instantaneous transition to 30% eHDVs results in on-road emission reductions that more than offset emission increases from EGUs (Fig. 1 and Supplementary Table 3). The highest-magnitude emission reductions occur along major road networks and within densely populated areas (Supplementary Fig. 9). Emission increases are limited to point sources within grid cells where EGUs reside (Fig. 1 and Supplementary Fig. 1) which are predominately gas-fired within our CTM domain (Fig. 1b). Despite an increase of -4.9 M tonnes of CO₂ per year at EGUs following an increase in electricity demand, we estimate net CO₂ emission reductions of -2.5 M tonnes per year. NO_x emissions also exhibit net reductions (-7%; Supplementary Table 3) compared with our baseline simulations in which HDVs are predominantly diesel powered—with the largest decreases along major traffic routes (Fig. 1a). Elemental carbon emissions show the second largest decrease following NO_x, with a net decrease of -6% (Supplementary Table 3). In contrast, SO₂ emissions, mostly emitted from coal combustion at EGUs⁴, increase by -3%. We note that the emission changes reported here are probably worst-case estimates as EGU emissions are projected to decrease as the grid continues to modernize and decarbonize³⁴.

Changes in NO₂ and O₃ concentrations

We find that the shift of 30% of HDVs to eHDVs results in domain-wide population-weighted NO₂ reductions of 0.5 ppb (-6%), with maximum reductions reaching 4.9 ppb (Fig. 2b). Reductions are particularly

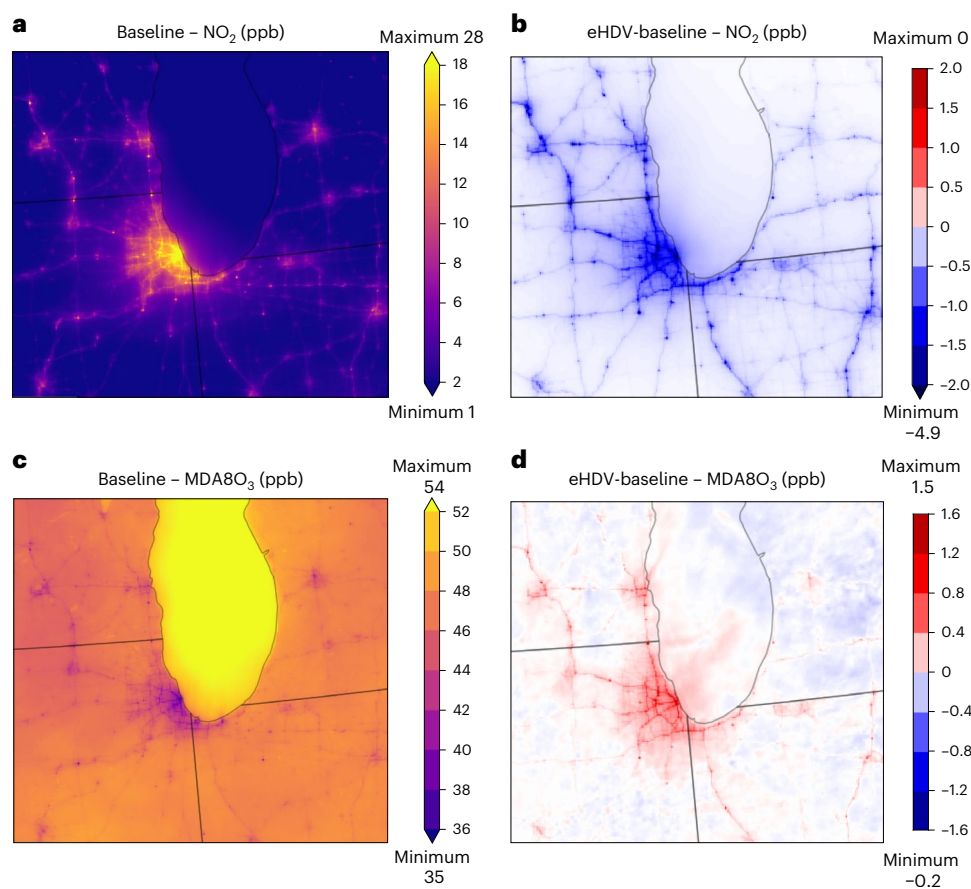


Fig. 2 | NO₂ and MDA8O₃ changes. **a–d**, Simulated annual mean (a) NO₂ and (c) MDA8O₃ baseline concentrations and differences in (b) NO₂ and (d) MDA8O₃ annual mean concentrations between the eHDV and baseline simulations.

pronounced along highway corridors, at transportation hubs, and within urban centres that also exhibit high baseline NO₂ concentrations (Fig. 2a and Supplementary Fig. 2) and NO_x emission reductions (Fig. 1a). In fact, NO₂ reductions in urban areas are ~3.5 times greater than reductions in rural regions (Fig. 2b and Supplementary Table 5). Even in grid cells containing EGUs, our simulations show net NO₂ reductions driven by on-road decreases, despite increased electricity demand and increased EGU NO_x emissions (Supplementary Table 4). Differences in NO₂ concentrations for individual simulated months are largely consistent with annual differences; however, larger-magnitude reductions are simulated in our summer and autumn months (Supplementary Fig. 3).

In contrast to NO₂ changes, annual mean daily maximum 8 h running mean O₃ concentrations (MDA8O₃)—a widely used regulatory and health-relevant O₃ metric—exhibit regionally mixed increases and decreases following eHDV adoption. We find increases in simulated MDA8O₃ concentrations of up to 1.45 ppb occurring adjacent to major highways and within urban areas (Fig. 2d and Supplementary Table 5) but decreases of up to 0.18 ppb in non-urban regions (Fig. 2d). However, domain average MDA8O₃ changes are positive (0.11 ppb; rural and 0.45 ppb; urban) with a population-weighted domain mean increase of 0.19 ppb (+0.4%). Areas exhibiting increases in simulated MDA8O₃ concentrations correspond to locations in the baseline with low MDA8O₃ but high NO₂ (Fig. 2a,c). On a seasonal basis, MDA8O₃ concentration changes are spatiotemporally heterogeneous (Supplementary Discussion and Supplementary Fig. 3).

Simulated patterns of heterogeneous change in MDA8O₃ concentrations can be explained by spatiotemporal variations in the O₃ regime, that is, the VOC-to-NO_x ratio. In highly polluted urban areas and along road networks we simulate low baseline surface VOC/NO_x

ratios (4.9 ppbC/ppb; Supplementary Table 6 and Supplementary Fig. 4), indicating a VOC-limited environment. Conversely, in rural and suburban areas, we simulate VOC/NO_x concentration ratios that are about twice those in urban areas, indicating NO_x-limited regimes (9.0 ppbC/ppb). Consequently, following eHDV adoption, NO_x reductions in urban and heavily trafficked areas lead to O₃ increases due to less titration of O₃ by NO (ref. 35). In addition, more OH radicals are available to react with VOCs, which in turn results in additional O₃ formation³⁶ (Supplementary Fig. 5). In rural and NO_x-limited areas, NO_x reductions have a marginal impact on the overall MDA8O₃ changes (-0.01 ppb; Fig. 2d). Our simulation of urban areas as NO_x-limited-to-transitional is consistent with previous studies^{33,37,38}. Prior work has suggested that the surface VOC/NO_x O₃ regime typically transitions around 8 ppbC/ppb; however, this threshold varies spatially and temporally and depends on factors such as local meteorology and VOC composition^{36,39}. In a nationwide study of O₃ regime surface VOC/NO_x ratios, Ashok and Barrett³⁷ estimate different ratios across the United States with -7 ppbC/ppb estimated for the Chicago Metropolitan Area, suggesting that ratios of less/more than 7 ppbC/ppb represent VOC-limited/NO_x-limited regimes. The seasonality of simulated MDA8O₃ changes can also be partially explained by VOC/NO_x ratios (Supplementary Discussion and Supplementary Table 6).

From a concentration threshold exceedance standpoint, electrification of 30% of on-road HDVs results in two to six additional grid cell days with MDA8O₃ levels higher than the World Health Organization's MDA8O₃ threshold exceedance guideline of 50 ppb (ref. 40) in urban areas such as Cook County, IL (home to Chicago; Fig. 3a) and Milwaukee, WI (Fig. 3b) as well as in isolated rural areas such as Noble County, IN (Fig. 3d). However, less of a clear signal is observed for counties in

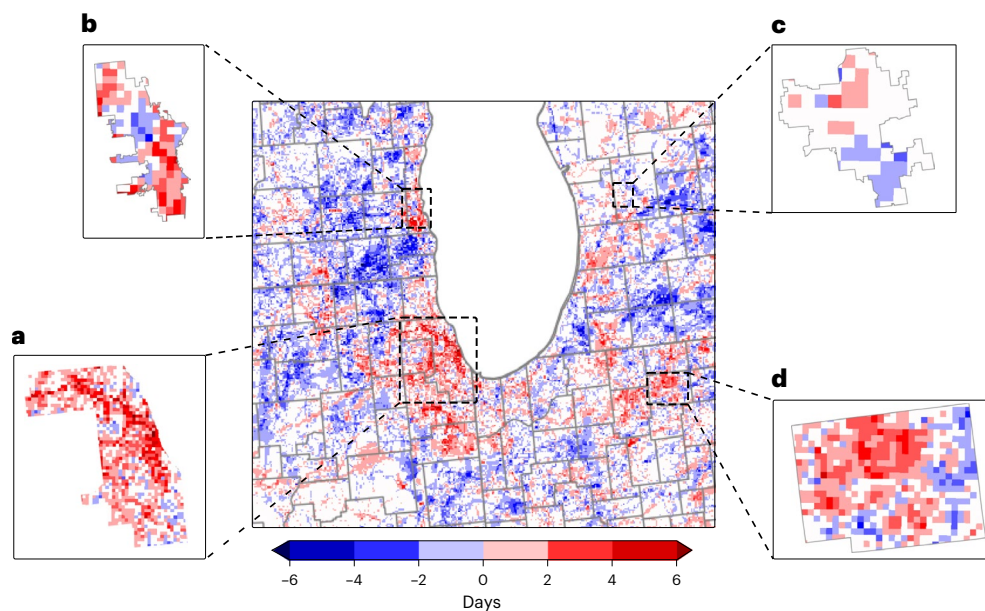


Fig. 3 | MDA8O₃ exceedances. **a–d**, Differences in number of grid cell days with MDA8O₃ levels greater than 50 ppb across the study domain and in Cook County, IL (**a**), Milwaukee, WI (**b**), Grand Rapids, MI (**c**) and Noble County, IN (**d**).

Michigan as we note both decreases and increases in the number of grid cell exceedance days (for example, Grand Rapids, MI; Fig. 3c). Applying the less stringent 70 ppb MDA8O₃ US EPA National Ambient Air Quality Standard results in 1–2 additional grid cell exceedance days mostly in north-western and southern Cook County (Supplementary Fig. 6).

Changes in PM_{2.5} concentrations

Thirty per cent adoption of eHDVs reduces annual mean population-weighted PM_{2.5} concentrations by an average of 0.09 $\mu\text{g m}^{-3}$ across the study domain and by a maximum of 0.49 $\mu\text{g m}^{-3}$ at hotspots within densely populated metropolitan areas—areas that generally have high simulated baseline PM_{2.5} concentrations (Fig. 4 and Supplementary Table 4). Although we note domain-wide decreases in PM_{2.5} concentrations (even in grid cells with EGUs), simulated sulfate (SO₄) concentrations increase in rural regions (Supplementary Fig. 7c). Sulfate and nitrate compete for ammonia⁴¹; therefore, as NO_x emissions decrease (−6.65%; Supplementary Table 3) and ammonia (NH₃) emissions remain largely unchanged (−0.02%; Supplementary Table 3), increases in SO₂ emissions (3.10%; Supplementary Table 3) result in decreases in NO₃ aerosols but increases in SO₄ aerosols (Supplementary Fig. 7). This PM chemical interplay highlights the utility of high-resolution CTMs to simulate the complex formation of air pollution not only at emission source locations such as EGUs but also in areas where secondary pollutants form, and exposure may occur.

Health benefits and trade-offs

To leverage the high spatial resolution of our simulated air quality changes, we utilize similarly high-resolution health data. When computed with census tract-level USALEEP baseline all-cause mortality data, domain-wide reductions in simulated annual mean NO₂ and PM_{2.5} concentrations for 30% eHDV adoption translate to 590 (95% confidence interval (CI) 150–900) and 70 (95% CI 20–110) annual avoided premature deaths compared with the baseline (Supplementary Table 7). We note that health benefits in urban areas such as Chicago do not occur at the expense of health damages in rural areas; even rural census tracts that contain EGUs experience health benefits. However, it should be noted that ~20% of the electricity demand is met by EGUs outside our CTM domain, where pollutant impacts cannot be assessed. In contrast to NO₂ and PM_{2.5}, the overall health impact associated with MDA8O₃

exposure across the domain adds up to 50 (95% CI 30–110) additional deaths per year. To exclude the influence of baseline mortality data, we also calculate the attributable fraction (equation (1)) and estimate that 0.42% and 0.05% decreases of all-cause baseline mortality are associated with reductions in NO₂ and PM_{2.5}, respectively, while a 0.04% increase of all-cause baseline mortality is associated with increases in annual mean MDA8O₃.

The spatial distribution of differences in attributable mortality rate (per 100,000) for each pollutant following eHDV adoption reflects both differences in simulated pollutant concentrations and underlying susceptibilities (Supplementary Fig. 8). We find that the highest differences in attributable mortality rates for all three pollutants occur in Cook County and along census tracts close to Interstate-90, which enters our domain on its eastern margin, passes just south of Lake Michigan, turns north-west across Cook County and exits the domain on its western margin (Supplementary Figs. 8 and 9). We note that the magnitude of air pollution changes does not scale linearly to the magnitude of estimated health impacts as pollutant exposure impacts depend on pollutant-specific β values as well as the spatial distribution of baseline mortality data. In fact, discrepancies between the spatial distribution of attributable mortality rate differences and air pollution concentrations, such as high mortality differences west of Cook County (Supplementary Fig. 8), are linked to the spatial variability of the baseline mortality data (Supplementary Fig. 10). That is, when census tracts with high baseline mortality rates coincide with moderate differences in pollutant concentrations, health impacts can be amplified as more susceptible people are exposed. Despite increases in estimated MDA8O₃-related attributable deaths, our results show that electrifying HDVs leads to health benefits largely resulting from substantial reductions in simulated NO₂ concentrations. The health estimates for related pollutants such as PM_{2.5} and NO₂ should be considered in isolation, as a summation of these health impacts could result in overestimated impacts⁹.

Equity implications

Resolving neighbourhood-scale pollutants not only allows us to distinguish differences in air pollution concentrations and their associated health impacts, but also facilitates an equity-focused analysis that characterizes racial/ethnic disparities in the air quality and public health

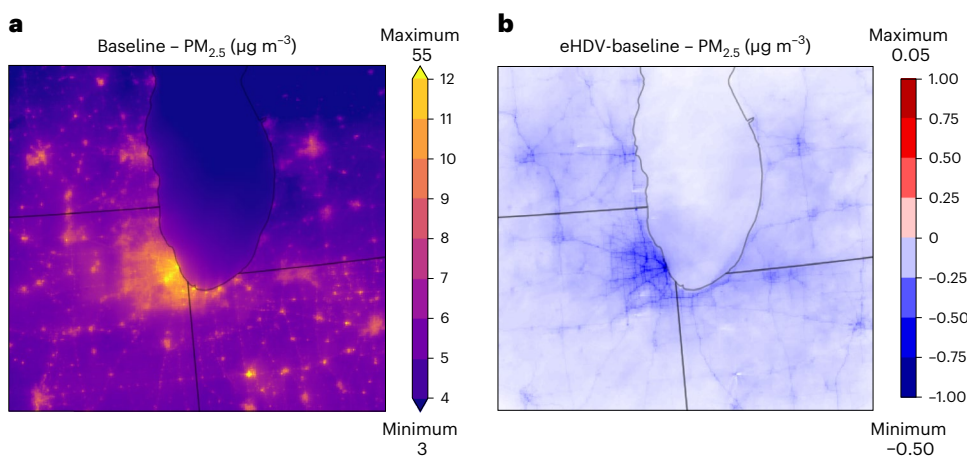


Fig. 4 | PM_{2.5} changes. a,b, Simulated annual mean PM_{2.5} baseline concentrations (a) and differences between the eHDV and baseline simulation (b).

benefits and trade-offs of eHDV adoption. Given its prodigious impact, we focus our eHDV equity analysis on NO₂, but provide PM_{2.5} and MDA8O₃ analyses in Supplementary Figs. 11 and 12. We assess the racial/ethnic composition of each NO₂ concentration change decile over the full model domain and within Chicago city limits (Fig. 5a,c). We also perform a similar analysis on changes in attributable mortality rate deciles (Fig. 5b,d). At the domain level, the largest NO₂ reductions (that is, highest magnitude pollutant decreases in the highest (10th) decile) occur where Black (24%), Asian (9%) and Hispanic or Latino (18%) populations represent a relatively high proportion of the total population within that decile (Fig. 5a), while the smallest reductions (that is, lowest magnitude decreases in the lowest (1st) decile) occur where non-Hispanic white populations predominate (90% of the population within the 1st decile Fig. 5a). Health benefits, in the form of reduced mortality rates, largely mirror NO₂ concentration declines; however, the Black population is overrepresented in the highest decile, indicating an outsized health benefit for this community (46%; Fig. 5b), largely driven by higher underlying baseline mortality rates and susceptibilities (Supplementary Fig. 10).

Within Chicago city limits, our equity findings are more nuanced. People of colour constitute the majority of the racial/ethnic composition for all Chicago NO₂ concentration change deciles (>50%; Fig. 5c). However, in contrast to our domain-level findings, NO₂ reductions are distributed more equally across population subgroups (Fig. 5c). This difference is reflective of the racial/ethnic make-up of the city and the proximity of non-Hispanic white populations to the northern branch of Interstate-90, where large reductions in NO₂ concentrations are simulated (Fig. 5e and Supplementary Fig. 13a). Despite relatively equitably distributed NO₂ reductions across population subgroups, we note disproportionately large NO₂-health benefits for Chicago's Black population, particularly in the higher (9th and 10th) deciles (43–68%; Fig. 5d). To help explain these outsized health impacts, we investigate the bivariate distribution of baseline mortality rates and simulated NO₂ changes across Chicago (Fig. 5e–g). Areas where NO₂ health benefits are greatest (Fig. 5f) correspond to census tracts with high baseline mortality rates and high NO₂ reductions (dark green; Fig. 5g), whereas areas with high NO₂ reductions and low baseline mortality rates (dark blue; Fig. 5g) experience lower health benefits (light green; Fig. 5f). Our results demonstrate that even low-to-moderate reductions in pollutant concentrations can lead to substantial health benefits (yellow; Fig. 5g); an outcome that is particularly true for Chicago's Black population whose spatial distribution (Supplementary Fig. 13b) only partially overlaps with high magnitude NO₂ reductions (Fig. 5f), but whose baseline mortality rates are relatively high. Indeed, we find that the spatial correlation of the City's Black population with the footprint of our simulated NO₂ reductions is relatively weak and

negative (Pearson's $r = -0.20$), whereas the Black population's correlations with NO₂ health benefits and baseline mortality rates are both higher and positive (Pearson's $r = 0.43$ and 0.54). This finding is consistent with previous studies that have demonstrated the outsized role of socio-demographic factors in determining health impacts as compared to pollutant exposure levels⁴².

Discussion

Using a regulatory-grade neighbourhood-resolving two-way coupled CTM, we demonstrate that net emissions decrease across our study domain (despite SO₂ emission increases at EGUs), leading to annual mean NO₂ and PM_{2.5} decreases of up to 4.91 ppb and 0.50 µg m⁻³, respectively. We highlight large decreases along dense road networks and in urban areas where on-road HDV emissions are highest. Reductions in on-road emissions outweigh increases in EGU emissions such that decreases in NO₂ and PM_{2.5} concentrations (and their associated health impacts) are simulated even in grid cells that contain EGUs. In contrast, we note increases in annual mean simulated MDA8O₃ concentrations in areas of high NO_x reductions and decreases in non-urban areas. Increases in MDA8O₃ concentrations are linked to a reduction in O₃ titration by NO as well as an increase in available OH radicals. Our results indicate that, in our domain, shifting to eHDVs increases VOC/NO_x ratios, which, if the shift is of a sufficient magnitude, could lead to a change in the O₃ regime of some areas, for example, areas in transition from VOC- to NO_x-limited, and could result in decreased O₃ formation following NO_x emission reductions of sufficient magnitude.

The overall impact of shifting emissions from on-road tailpipes and refuelling infrastructure to EGUs largely depends on the electricity generation mix of the region as well as the distribution of electricity from EGUs to sources of demand^{43,44}. The predominant electricity generation mix in our domain is natural gas. As such, results presented in this study, particularly results pertinent to emission changes at EGUs and changes in PM_{2.5} concentrations, might differ when looking at regions with a different electricity generation mix, when incorporating a decarbonizing electric grid⁴⁵, or when using Earth System simplifying RCMs⁴⁶. Nonetheless, results presented in this study are largely consistent with previous studies that have focused on changes in air pollutant concentrations following the adoption of various EVs scenarios. Previous CTM-based studies suggest that transitioning to EVs leads to reductions in net NO_x emissions despite projected increases in electricity demand^{26,29}. Similarly, previous United States-focused studies employing different EV adoption scenarios have shown reductions in PM_{2.5} concentrations both nationwide^{29,31} and regionally²⁶. Using 12 km CTM United States-wide simulations and shifting 17% of light-duty vehicles and 8% of HDVs to electric, Nopmongcol et al.²⁹

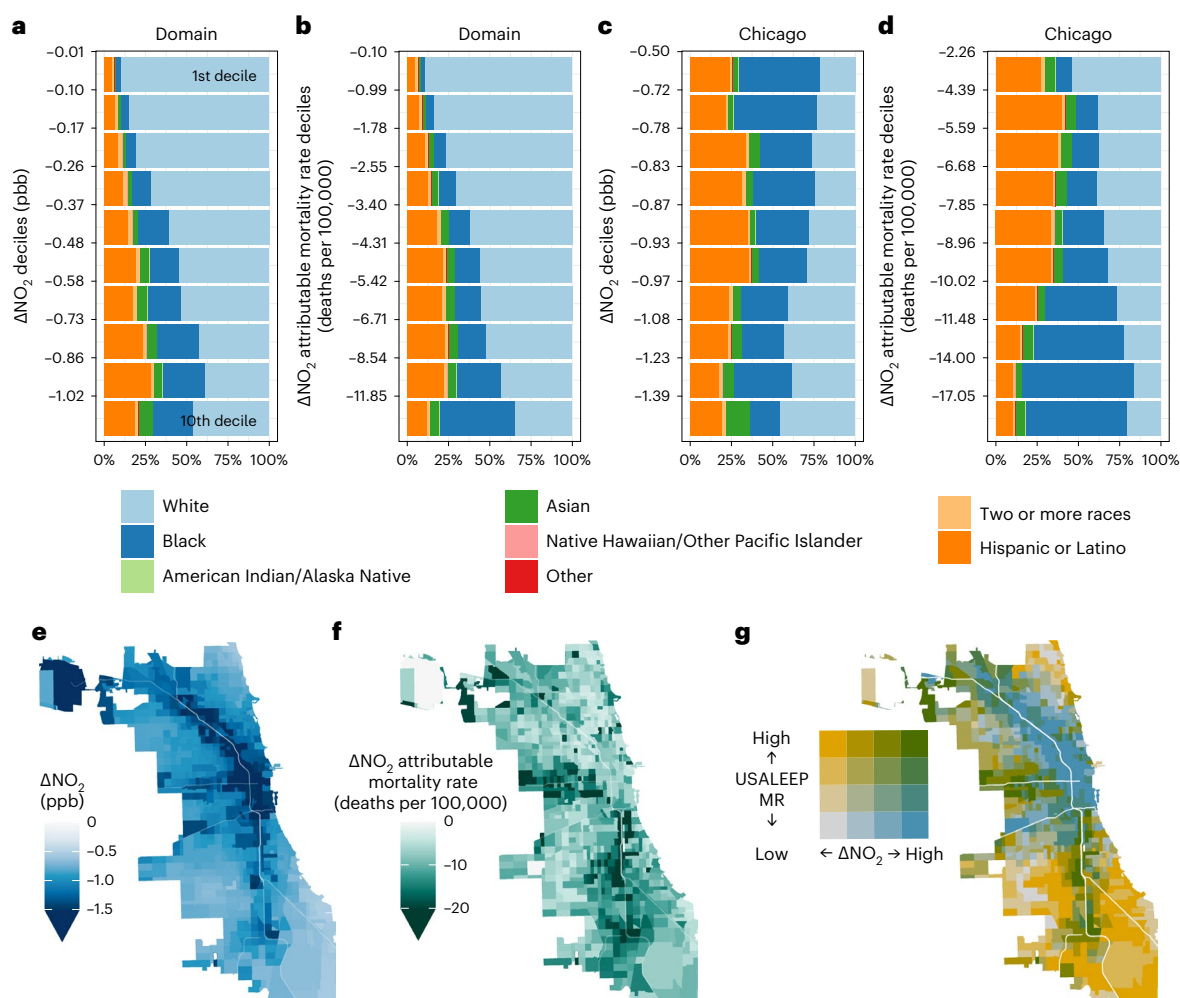


Fig. 5 | Equity Implications of eHDV adoption. a–d, Fractional race and ethnicity of populations for deciles of NO₂ concentration changes (a and c) and NO₂ attributable mortality rate changes (b and d) for the full model domain (a and b) and the city of Chicago (c and d) with 30% eHDV adoption. Decile ranks

indicated on a. e–g, Highlight of city of Chicago NO₂ concentration changes (e), NO₂ attributable mortality rate changes (f) and bivariate depiction of the relationship of baseline USALEEP mortality rates with NO₂ changes (g). All race groups except Hispanic or Latino, include only those identifying as non-Hispanic.

found PM_{2.5} reductions of less than 0.5 μg m⁻³ for most of the eastern United States despite a projected 5% increase in electricity demand, met mostly by natural gas. In contrast, Schnell et al.³¹, using a 50 km CTM, found somewhat mixed results for the United States, that is, with 25% electric light-duty vehicle adoption PM_{2.5} benefits/disbenefits were strongly dependent on the region and season, with a high sensitivity to a region's electricity generation mix. Lastly, when comprehensive fleet turnover to EVs was assessed using a CTM with 1 km resolution over the Greater Houston area, Pan et al.²⁶ found PM_{2.5} reductions ranging between 0.5 and 2 μg m⁻³ with large reductions near highways.

Changes in O₃ concentrations driven by the adoption of different classes of EVs have also been reported; however, results are varied. Nationwide studies using CTMs at medium-to-coarse resolutions report widespread reductions in O₃ (refs. 29,31) largely driven by on-road NO_x emission reductions³¹. However, Schnell et al.³¹ observed O₃ increases in some grid cells, for example, in southern California and north-eastern Illinois. More regionally focused CTM studies at finer scales^{26,32} also found increases in O₃ concentrations, particularly along highways and in NO_x-saturated environments. Consistent with results presented in this study, increases in O₃ in these more regionally focused studies are generally linked to smaller reductions in VOC emissions as compared with NO_x emission reductions in NO_x-saturated environments leading to reduced O₃ titration by NO (refs. 26,32). The differences in O₃ responses

to EV adoption summarized here may be related to differences in study design, simulated domain and/or model configuration and complexity, although it is notable that increases in spatial resolution tend to demonstrate pockets of increasing O₃ concentrations with EV adoption, suggesting that resolving fine-scale features is critical to resolving non-linear chemistry and the formation of secondary pollutants over tight spatial gradients (for example, near roadways or in urban environments), and is particularly critical for studies focused on public health impacts and/or environmental justice outcomes.

Accurately representing the environmental impacts of EV adoption scenarios is limited by our ability to forecast EV market share as well as the future evolution of the US electric grid. Projections for EV sales continue to increase from a 2018 estimate of 21% of new car sales to a recent estimate of 52% by 2030 (ref. 47). Our 30% eHDV instantaneous adoption estimate should not be considered a forecast with a specific time horizon. Indeed, our use of 2016 grid infrastructure with 30% eHDV adoption is temporally inconsistent, and the air quality benefits and trade-offs tied to grid infrastructure reported here should be considered conservative, given the on-going transition of current grid infrastructure to emission-free EGUs⁴⁸. To quantify the sensitivity of our results to a future grid, we run sensitivity simulations assuming all added grid demand from 30% eHDV adoption is met by emission-free EGUs. We find that over our domain, average NO₂, PM_{2.5} and MDA8O₃

concentrations decrease further when the additional electricity demand needed for charging is supplied by emission-free sources (-0.17% , -0.09% and -0.004% , respectively). These relatively small magnitude changes highlight the marginal impact of EGU emissions on air quality as compared with on-road emissions when transitioning to EVs. While we account for emissions related to hotelling trucks, which represent the hours truck drivers spend in their long-haul trucks during mandated rest periods⁴⁹, the emissions modelling scheme used in this study does not include HDV idling emissions during loading/unloading or queuing at warehouses. Future eHDV studies should incorporate these emission processes as they might amplify the net effect of eHDVs, particularly for communities living near such facilities. Here we present changes in eHDV on-road tailpipe and refuelling emissions; however, we do not consider any increased contributions to on-road non-exhaust emissions such as brake wear, tyre wear, road wear and road dust resuspension that contribute to on-road PM and that might increase in the future as heavy batteries in EVs weigh more compared with internal combustion engines, particularly for vehicles with a larger driving range⁵⁰. Lastly, here we choose to electrify only HDVs to isolate and characterize eHDV adoption impacts. However, the transition to electrified transport will not occur in isolation, but rather will co-occur with other vehicle classes, different alternative fuel transportation technologies (for example, hydrogen), changes in fuel refining infrastructure, scale-up of battery manufacturing, and changes in other forms of emitting infrastructure (for example, heating, ventilation and air conditioning systems (HVACs), cooking stoves, urban greening and so on).

Despite the above caveats, our results demonstrate that transitioning 30% of HDVs to eHDVs has robust air quality and health benefits, including reduced NO₂ and PM_{2.5} concentrations and associated health benefits, reduced air pollution disparities among population subgroups, and reduced CO₂ emissions. To contextualize the CO₂ changes in terms of their economic damages and/or benefits we use a state-of-the-science social cost of carbon estimate of \$185 per tonne of CO₂ (\$44–413 per t-CO₂; 5–95% range, 2020 US dollars⁵¹), in line with an EPA-proposed estimate currently under review⁵². Multiplying the 30% eHDV net CO₂ reduction (-2.5 Mt per year) by the social cost of carbon, we estimate net savings of \$456M per year within our domain. However, this estimate is based on the 2016 grid and therefore should be considered conservative. Assuming a best-case scenario whereby all the additional electricity demand needed for charging eHDVs is met by renewable resources, the avoided CO₂-related damage costs following 30% eHDV adoption would increase to \$1.4B per year. For ease of comparison, we also estimate monetized health impacts, by multiplying the widely used estimate of value of a statistical life of \$9.6M (ref. 53) by the estimated traffic-related avoided or additional attributable deaths from eHDV adoption. With current grid infrastructure and 30% eHDV adoption, we estimate \$5.7B and \$0.6B in avoided annual health damages related to NO₂ and PM_{2.5} reductions and an additional cost of \$0.5B yearly related to MDA8O₃ increases. Supplying the additional electricity demand to charge 30% of HDVs from emission-free electricity sources could result in additional savings associated with NO₂ and PM_{2.5} avoided health damages ($-\$97$ M (NO₂) and $\$67$ M (PM_{2.5})) while health damages associated with MDA8O₃ remain unaltered. Our results show higher monetized savings associated with mortality co-benefits as compared with savings associated solely with CO₂ reductions. This finding agrees with studies suggesting air quality co-benefits of similar magnitude to abatement cost estimates^{54,55} and emerging literature showing that health co-benefits not only offset the cost of climate action but exceed it⁵⁶.

In this study, use of a neighbourhood-resolving CTM has allowed us to simulate changes in both primary and secondary pollutants and characterize air quality and public health benefits and trade-offs at equity-relevant scales. The methods used here demonstrate the ability of Earth-system-science tools to assess the benefits, trade-offs and

equity implications of proposed climate solutions at the scales envisioned by recent aspirational policy proposals. While computational expense limits our domain of focus, our work has global implications, and demonstrates that policies aimed at reducing transportation emissions could have unintended consequences, such as increases in secondary pollutants like O₃. Regulatory consequences hinging on single pollutants can mask overall air quality benefits which are better addressed by holistic air quality measures. Consequently, here we show that a shift to greener HDVs has the potential to improve overall air quality and reduce health burdens, especially in marginalized communities.

Methods

Air quality model set-up and eHDV emission scenarios

To simulate changes in air pollution that result from eHDV adoption, we use the two-way coupled Community Multi-scale Air Quality (CMAQ, v5.2 (ref. 57)) and Weather Research and Forecasting (WRF, v3.8 (ref. 58)) modelling system (WRF-CMAQ⁵⁹). Our analysis domain has a 1.3 km horizontal resolution, is centred on southern Lake Michigan (Fig. 1a), encompasses parts of WI, IL, IN and MI, and includes the urban centres of Chicago, IL, Milwaukee, WI, and Grand Rapids, MI. One month baseline, that is, no-eHDVs and no EGU changes, WRF-CMAQ simulations were performed and validated for each meteorological season (August and October 2018, and January and April 2019). Details of these baseline simulations together with WRF-CMAQ performance metrics can be found in Supplementary Table 1 and Discussion, and in Montgomery et al.⁶⁰. We note that pollutant concentrations are highly dependent on meteorological conditions and given the temporally limited scope of our simulations, interpretation of results should bear this in mind⁶¹. Annual means presented in this study represent the average of the four simulated months, similar to previous resource-intensive CTM studies (for example, Peng et al.⁶²).

Meteorologically informed 1.3 km emissions for the baseline and eHDV scenario simulations were created using the Sparse Matrix Operator Kernel Emissions (SMOKE) processing system⁶³ with the EPA's Beta platform⁶⁴ in conjunction with emission factors from the Motor Vehicle Emission Simulator (MOVES)⁴⁹. HDV processes captured in MOVES include: running and start exhaust, brake wear and tyre wear, evaporative emissions, crankcase exhaust, refuelling emissions and extended idling (that is, hotelling) emissions. MOVES generates four types of emissions factors: rate-per-distance, rate-per-vehicle, rate-per-profile and rate-per-hour. Emissions factors take into consideration vehicle type (for example, passenger car, heavy-duty truck and so on; Supplementary Table 3), age distribution of vehicle type fleet, road type and vehicle type usage (that is, class of roadway), and ambient meteorology⁶⁵. The SMOKE emissions model then combines activity data (for example, vehicle miles travelled (VMT) and vehicle population), meteorological data, MOVES emission factors and other ancillary data, such as speed distributions, to generate hourly, meteorologically adjusted mobile emissions⁶⁶. County total emissions from the 2016v7.2 National Emissions Inventory (NEI)⁶⁴ were processed using the 2016 SMOKE Beta platform in conjunction with 1.3 km spatial surrogates provided by the Lake Michigan Air Directors Consortium⁶⁷. Spatial surrogates allocate NEI county-level emission estimates to model grid cells (1.3 km) using spatially resolved land use information specific to the study domain (for example, population, industry, location of roadways and so on). The fractional composition of spatial surrogates within each grid cell is used as a proxy to refine county-level emissions to finer scales⁶⁵ (refer also to Supplementary Discussion). Using SMOKE, we calculate anthropogenic on-road, point, and area emissions, while biogenic (BEIS), lightning NO_x and windblown dust emissions were calculated interactively within CMAQ.

In our eHDV scenario, we instantaneously transition 30% of internal combustion engine HDVs to eHDVs (that is, unaccompanied by any decarbonization shifts in the power sector and a 1-to-1 on-road fleet replacement with no shift from on-road freight to, for example,

rail). This 30% target falls within the decarbonization mid-transition, a period in which our reliance on fossil-fuelled EGUs remains critical⁶⁸. For the eHDV scenario we scale down the annual county-level VMTs for each HDV type, that is, intercity, transit and school buses; refuse, single-unit short-haul and single-unit long-haul trucks, motor homes, combination short-haul and long-haul trucks by 30% (Supplementary Table 2). HDV emissions for all MOVES processes are reduced by 30% through modification of emissions factor tables (EFTABLES) in SMOKE. The increase in EGU electricity demand was estimated at the county level as a function of VMTs that are now electric, vehicle type charging efficiency, and a grid gross loss of 5.1% (ref. 69) (supplementary equation 1). We estimate the increase in electricity demand at EGUs using an augmented version of the vehicle-to-EGU electricity assignment algorithm employed by Schnell et al.^{31,45}. Emission changes at EGUs are computed at the CONUS level from which the changes occurring at EGUs within our CTM domain are selected. As such this study does not consider changes in air quality and associated health and equity impacts at EGUs outside our CTM domain. Presuming an instantaneous increase in demand, the augmented version of the emission remapping algorithm uses 2016 grid infrastructure and is described in detail in Supplementary Discussion, although we also discuss simulations whereby the increase in electricity demand is sourced from emission-free electricity generation in the discussion. We run month-long eHDV simulations and compare results with simulations in which HDVs are predominantly diesel powered (baseline). Throughout this study, differences between the baseline and the eHDV simulations are presented as eHDV–baseline such that negative changes represent lower values for the eHDV scenario as compared with the baseline simulations and vice versa.

Health and equity impacts

Changes in all-cause mortality associated with differences in annual mean NO₂ and PM_{2.5} and daily maximum 8 h running mean O₃ (MDA8O₃) between the baseline and eHDV scenarios were estimated at the census tract level using the following equations:

$$AF_{CT} = 1 - \exp(-\beta\Delta x_{CT}) \quad (1)$$

$$Mort_{CT} = BMR_{CT} \times POP_{CT} \times AF_{CT} \quad (2)$$

The attributable fraction (AF_{CT}) is estimated following equation (1) where Δx_{CT} represents the simulated changes in annual mean air pollution concentrations between the baseline and eHDV scenario at the census tract level (CT). We note that annual mean air pollution levels are an average of the four simulation months from each meteorological season. Census tract-level air pollution concentrations were determined by calculating the area average of the intersection between grid cell-level simulated pollutant concentrations and census tract polygons (using the GeoPandas package⁷⁰). β is a coefficient derived from epidemiological studies describing the relationship between the specific air pollutant and the associated health outcome. For each census tract, the all-cause mortality is then estimated by multiplying the AF by the baseline mortality (equation (2)). The baseline mortality for each census tract is calculated by multiplying the population within each census tract (POP_{CT}) by the corresponding baseline mortality rate (BMR_{CT}). Age-stratified census tract-level population and demographic data were obtained from the American Community Survey (ACS 2015–2019) (ref. 71). We have specifically used 5 year estimates from 2015–2019 as these include a larger sample size thereby reducing the margin of error as compared with datasets spanning a shorter time period. To maintain a high level of detail through our health estimates, we also use recent census tract-level age-specific all-cause baseline mortality rates obtained from Industrial Economic, Incorporated with different rates for each 5 year age group (IEc 2010–2015) (ref. 72). These mortality incidence rates are derived from

USALEEP abridged life tables with modifications for broader use in national health benefits analyses.

For our NO₂ and PM_{2.5} health estimates we use β values derived from the latest Health Effects Institute systematic review and meta-analysis report assessing long-term traffic-related health effects⁹ and for O₃ we use β values derived from an extended analysis of the Cancer Prevention Study II by Turner et al.⁷³. All-cause mortality associated with long-term exposure to NO₂ is estimated using a relative risk (RR) of 1.04 (95% CI 1.01–1.06 (ref. 9)) per 10 $\mu\text{g m}^{-3}$ converted to ppb equivalent using our model simulated annualized mean temperature of 9.4 °C (ref. 60) (that is, 10 $\mu\text{g m}^{-3}$ = 5.04 ppb NO₂ translating to a β value of -0.008). An RR of 1.02 (95% CI 1.01–1.04 (ref. 73)) per 10 ppb is then used to estimate the all-cause mortality associated with long-term exposure to MDA8O₃. Finally, to estimate the PM_{2.5}-related health impacts we use an RR of 1.03 (95% CI 1.01–1.04 (ref. 9)) per 5 $\mu\text{g m}^{-3}$. The exposure estimates presented in this study hold for the population 30 years and older. Given the different sources used for each RR, and the underlying differences in methodologies, we do not present summed health estimates of the three pollutants as a combined estimate could lead to a misrepresentation of the true effect.

Reporting summary

Further information on research design is available in the Nature Portfolio Reporting Summary linked to this article.

Data availability

As inputs to our Vehicle-to-EGU Electricity Assignment and Emission Remapping Algorithm we use: a grid gross loss across the United States from EPA (2021) (refs. 69), the eGRID-2016 database⁷⁴ for EGU details related to location, age and capacity with shapefiles from US Census Cartographic boundary shapefiles⁷⁵ and NERC⁷⁶. Model output is hosted on Northwestern's servers. Due to model output size limitation, specific model output requests can be made to the corresponding author. For our health and equity impacts, population and demographic data was obtained from the American Community Survey (ACS 2015–2019 (ref. 71)) and can be downloaded from <https://doi.org/10.18128/D050.V17.0>, baseline all-cause mortality incidence rates were obtained from Industrial Economic, Incorporated (IEc 2010–2015) (ref. 72) and are available on request, β values are obtained from latest Health Effects Institute systematic review and meta-analysis report⁹ and for O₃ β values are from an extended analysis of the Cancer Prevention Study II by Turner et al.⁷³.

Code availability

The WRF-CMAQ two-way model source code used for this numerical model study can be downloaded for WRF at https://www2.mmm.ucar.edu/wrf/users/download/get_sources.html and for CMAQ at <https://github.com/USEPA/CMAQ>. Simulations were conducted using WRF-CMAQ v5.2 and WRF v3.8. The 2016 SMOKE Beta platform was used for allocating emissions to a 1.3 km grid with county total emissions from the 2016v7.2 NEI and 1.3 km spatial surrogate provided by the Lake Michigan Air Directors Consortium (LADCO) and available on request. The code used for our Vehicle-to-EGU Electricity Assignment and Emission Remapping Algorithm can be found at https://github.com/NU-CCRG/Camilleri-et-al-2022_WRF-CMAQ-eHDVstudy. All analysis was conducted using R Version 4.2.2, Python Version 3.8.12 with the GeoPandas package for determining census tract-level air pollution concentrations Version 0.9.0 and Microsoft Excel Version 16.66.1. State boundaries are obtained using Cartopy v0.18.0 (<https://doi.org/10.5281/zenodo.8216315>), while Chicago shapefiles are available from the Chicago Data Portal via <https://data.cityofchicago.org/>. All data analysis scripts including those used for estimating health and equity implication are available at <https://doi.org/10.5281/zenodo.8234544>.

References

1. *Clean Trucks, Clean Air, American Jobs* (EDF, 2021).
2. *Clean Truck Plans—Regulatory Update (EPA-420-F-21-057)* (EPA, 2021).
3. Delivering clean air: health benefits of zero-emission trucks. *American Lung Association* <https://www.lung.org/getmedia/e1ff935b-a935-4f49-91e5-151f1e643124/zero-emission-truck-report.pdf> (2022).
4. Inventory of U.S. Greenhouse Gas Emissions and Sinks: 1990–2020, EPA 430-R-22-003. *EPA* <https://www.epa.gov/ghgemissions/draft-inventory-us-greenhouse-gas-emissions-2022> (2022).
5. Shah, R. U. et al. High-spatial-resolution mapping and source apportionment of aerosol composition in Oakland, California, using mobile aerosol mass spectrometry. *Atmos. Chem. Phys.* **18**, 16325–16344 (2018).
6. Davidson, K., Fann, N., Zawacki, M., Fulcher, C. & Baker, K. R. The recent and future health burden of the U.S. mobile sector apportioned by source. *Environ. Res. Lett.* **15**, 075009 (2020).
7. Anenberg, S. C., Miller, J., Henze, D. K., Minjares, R. & Achakulwisut, P. The global burden of transportation tailpipe emissions on air pollution-related mortality in 2010 and 2015. *Environ. Res. Lett.* <https://doi.org/10.1088/1748-9326/ab35fc> (2019).
8. Anenberg, S. C. et al. Long-term trends in urban NO₂ concentrations and associated paediatric asthma incidence: estimates from global datasets. *Lancet Planet. Health* **6**, e49–58 (2022).
9. *Systematic Review and Meta-analysis of Selected Health Effects of Long-Term Exposure to Traffic-Related Air Pollution. Special Report 23* (HEI, 2022).
10. Chang, S. Y. et al. A modeling framework for characterizing near-road air pollutant concentration at community scales. *Sci. Total Environ.* **538**, 905–921 (2015).
11. Apte, J. S. et al. High-resolution air pollution mapping with google street view cars: exploiting big data. *Environ. Sci. Technol.* **51**, 6999–7008 (2017).
12. Caubel, J. J., Cados, T. E., Preble, C. V. & Kirchstetter, T. W. A distributed network of 100 black carbon sensors for 100 days of air quality monitoring in West Oakland, California. *Environ. Sci. Technol.* **53**, 7564–7573 (2019).
13. Research on near roadway and other near source air pollution. *EPA* <https://www.epa.gov/air-research/research-near-roadway-and-other-near-source-air-pollution> (2020).
14. Rowangould, G. M. A census of the US near-roadway population: public health and environmental justice considerations. *Transp. Res. D* **25**, 59–67 (2013).
15. Colmer, J., Hardman, I., Shimshack, J. & Voorheis, J. Disparities in PM_{2.5} air pollution in the United States. *Science* **369**, 575–578 (2020).
16. Castillo, M. D. et al. Estimating intra-urban inequities in PM_{2.5}-attributable health impacts: a case study for Washington, DC. *Geohealth* **5**, e2021GH000431 (2021).
17. Kerr, G. H., Goldberg, D. L. & Anenberg, S. C. COVID-19 pandemic reveals persistent disparities in nitrogen dioxide pollution. *Proc. Natl Acad. Sci. USA* **118**, e2022409118 (2021).
18. Chambliss, S. E. et al. Local- and regional-scale racial and ethnic disparities in air pollution determined by long-term mobile monitoring. *Proc. Natl Acad. Sci. USA* **118**, e2109249118 (2021).
19. Fuller, C. H. & Brugge, D. in *Traffic-Related Air Pollution* (eds Khreis, H. et al.) 495–510 (Elsevier, 2020).
20. Clark, L. P., Harris, M. H., Apte, J. S. & Marshall, J. D. National and intraurban air pollution exposure disparity estimates in the United States: impact of data-aggregation spatial scale. *Environ. Sci. Technol. Lett.* <https://doi.org/10.1021/acs.estlett.2c00403> (2022).
21. JUSTICE40 a whole-of-government initiative. *The White House* <https://www.whitehouse.gov/environmentaljustice/justice40/> (2022).
22. Choma, E. F., Evans, J. S., Hammitt, J. K., Gómez-Ibáñez, J. A. & Spengler, J. D. Assessing the health impacts of electric vehicles through air pollution in the United States. *Environ. Int.* **144**, 106015 (2020).
23. Goodkind, A. L., Tessum, C. W., Coggins, J. S., Hill, J. D. & Marshall, J. D. Fine-scale damage estimates of particulate matter air pollution reveal opportunities for location-specific mitigation of emissions. *Proc. Natl Acad. Sci. USA* **116**, 8775–8780 (2019).
24. Tessum, C. W., Hill, J. D. & Marshall, J. D. InMAP: a model for air pollution interventions. *PLoS ONE* **12**, e0176131 (2017).
25. Thakrar, S. K. et al. Global, high-resolution, reduced-complexity air quality modeling for PM_{2.5} using InMAP (Intervention Model for Air Pollution). *PLoS ONE* **17**, e0268714 (2022).
26. Pan, S. et al. Potential impacts of electric vehicles on air quality and health endpoints in the Greater Houston Area in 2040. *Atmos. Environ.* **207**, 38–51 (2019).
27. Li, N. et al. Potential impacts of electric vehicles on air quality in Taiwan. *Sci. Total Environ.* **566–567**, 919–928 (2016).
28. Gai, Y. et al. Health and climate benefits of electric vehicle deployment in the greater Toronto and Hamilton area. *Environ. Pollut.* **265**, 114983 (2020).
29. Nopmongcol, U. et al. Air quality impacts of electrifying vehicles and equipment across the United States. *Environ. Sci. Technol.* **51**, 2830–2837 (2017).
30. Peters, D. R., Schnell, J. L., Kinney, P. L., Naik, V. & Horton, D. E. Public health and climate benefits and trade-Offs of U.S. vehicle electrification. *Geohealth* **4**, e2020GH000275 (2020).
31. Schnell, J. L. et al. Air quality impacts from the electrification of light-duty passenger vehicles in the United States. *Atmos. Environ.* **208**, 95–102 (2019).
32. Brinkman, G. L., Denholm, P., Hannigan, M. P. & Milford, J. B. Effects of plug-in hybrid electric vehicles on ozone concentrations in Colorado. *Environ. Sci. Technol.* **44**, 6256–6262 (2010).
33. Koplitz, S. et al. Changes in ozone chemical sensitivity in the United States from 2007 to 2016. *ACS Environ. Au* <https://doi.org/10.1021/acsenvironau.1c00029> (2021).
34. Grubert, E. Fossil electricity retirement deadlines for a just transition. *Science* **370**, 1171–1173 (2020).
35. Monks, P. S. et al. Atmospheric composition change—global and regional air quality. *Atmos. Environ.* **43**, 5268–5350 (2009).
36. National Research Council. *Rethinking the Ozone Problem in Urban and Regional Air Pollution. Rethinking the Ozone Problem in Urban and Regional Air Pollution* (National Academies Press, 1991).
37. Ashok, A. & Barrett, S. R. H. Adjoint-based computation of U.S. nationwide ozone exposure isopleths. *Atmos. Environ.* **133**, 68–80 (2016).
38. Jin, X. et al. Inferring changes in summertime surface ozone-NO_x-VOC chemistry over U.S. urban areas from two decades of satellite and ground-based observations. *Environ. Sci. Technol.* **54**, 6518–6529 (2020).
39. Seinfeld, J. H. & Pandis, S. N. *Atmospheric Chemistry and Physics from Air Pollution to Climate Change* (John Wiley & Sons, 2006).
40. *WHO Global Air Quality Guidelines. Particulate Matter (PM_{2.5} and PM₁₀), Ozone, Nitrogen Dioxide, Sulfur Dioxide and Carbon Monoxide* (WHO, 2021).
41. Pye, H. O. T. et al. Effect of changes in climate and emissions on future sulfate-nitrate-ammonium aerosol levels in the United States. *J. Geophys. Res. Atmos.* **114**, 138385 (2009).
42. Yang, H., Huang, X., Westervelt, D. M., Horowitz, L. & Peng, W. Socio-demographic factors shaping the future global health burden from air pollution. *Nat. Sustain.* <https://doi.org/10.1038/s41893-022-00976-8> (2022).

43. Huo, H., Cai, H., Zhang, Q., Liu, F. & He, K. Life-cycle assessment of greenhouse gas and air emissions of electric vehicles: a comparison between China and the U.S. *Atmos. Environ.* **108**, 107–116 (2015).
44. Lin, W. Y. et al. Analysis of air quality and health co-benefits regarding electric vehicle promotion coupled with power plant emissions. *J. Clean Prod.* **247**, 119152 (2020).
45. Schnell, J. L. et al. Potential for electric vehicle adoption to mitigate extreme air quality events in China. *Earths Future* **9**, e2020EF001788 (2020).
46. Holland, S. P., Mansur, E. T., Muller, N. Z. & Yates, A. J. Are there environmental benefits from driving electric vehicles? The importance of local factors. *Am. Econ. Rev.* **106**, 3700–3729 (2016).
47. Najman, L. EV adoption in US is happening faster than predicted. *RECURRENT* <https://www.recurrentauto.com/research/ev-adoption-us> (2022).
48. Grubert, E. Emissions projections for US utilities through 2050. *Environ. Res. Lett.* **16**, 084049 (2021).
49. *Motor Vehicle Emission Simulator (MOVES): User Guide for MOVES2014 (EPA-420-B-14-055)* (EPA, 2014).
50. Non-exhaust particulate emissions from road transport: an ignored environmental policy challenge. *OECD* <https://www.oecd-ilibrary.org/sites/4a4dc6ca-en/index.html?itemId=/content/publication/4a4dc6ca-en#execsumm-d1e285>, <https://doi.org/10.1787/4a4dc6ca-en> (2020).
51. Rennert, K. et al. Comprehensive evidence implies a higher social cost of CO₂. *Nature* <https://doi.org/10.1038/s41586-022-05224-9> (2022).
52. *Report on the Social Cost of Greenhouse Gases: Estimates Incorporating Recent Scientific Advances (Draft)* (EPA, 2022).
53. Anenberg, S. C., Miller, J., Henze, D. & Minjares, R. A global snapshot of the air pollution-related health impacts of transportation sector emissions in 2010 and 2015. *ICCT* www.theicct.org (2019).
54. Nemet, G. F., Holloway, T. & Meier, P. Implications of incorporating air-quality co-benefits into climate change policymaking. *Environ. Res. Lett.* **5**, 014007 (2010).
55. Li, M. et al. Air quality co-benefits of carbon pricing in China. *Nat. Clim. Chang* **8**, 398–403 (2018).
56. Shindell, D. et al. Temporal and spatial distribution of health, labor, and crop benefits of climate change mitigation in the United States. *Proc. Natl Acad. Sci. USA* **118**, e2104061118 (2021).
57. Byun, D. & Schere, K. L. Review of the governing equations, computational algorithms, and other components of the models-3 Community Multiscale Air Quality (CMAQ) modeling system. *Appl. Mech. Rev.* <https://doi.org/10.1115/1.2128636> (2006).
58. Skamarock, W. C. et al. A description of the advanced research WRF version 3 (no. NCAR/TN-475+STR). *OpenSky* <https://doi.org/10.5065/D68S4MVH> (2008).
59. Wong, D. C. et al. WRF-CMAQ two-way coupled system with aerosol feedback: software development and preliminary results. *Geosci. Model Dev.* **5**, 299–312 (2012).
60. Montgomery, A., Schnell, J. L., Adelman, Z., Janssen, M. & Horton, D. E. Simulation of neighborhood-scale air quality with two-way coupled WRF-CMAQ over Southern Lake Michigan-Chicago Region. *J. Geophys. Res. Atmos.* <https://doi.org/10.1029/2022JD037942> (2023).
61. Garcia-Menendez, F., Monier, E. & Selin, N. E. The role of natural variability in projections of climate change impacts on U.S. ozone pollution. *Geophys. Res. Lett.* **44**, 2911–2921 (2017).
62. Peng, L. et al. Alternative-energy-vehicles deployment delivers climate, air quality, and health co-benefits when coupled with decarbonizing power generation in China. *One Earth* **4**, 1127–1140 (2021).
63. Baek, B. H. & Seppanen, C. bokhaeng/SMOKE: SMOKE v4.5 Public Release (April 2017) (SMKOE v45_Apr2017). *Zenodo* <https://zenodo.org/record/1321280#YulGK-xBx44> (2018).
64. Eyth, A., Vukovich, J., Farkas, C. & Strum, M. Technical Support Document (TSD): preparation of emissions inventories for the version 7.2 - 2016 North American Emissions Modeling Platform. *EPA* https://www.epa.gov/sites/default/files/2019-09/documents/2016v7.2_regionalhaze_emismod_tsd_508.pdf (2019).
65. SMOKE-MOVES and the Emissions Modeling Framework. *CMAS* https://www.cmascenter.org/emf/internal/smoke_moves/ (2015).
66. *SMOKE v4.5 User's Manual* (UNC-Chapel Hill, 2017); https://www.cmascenter.org/smoke/documentation/4.5/manual_smokev45.pdf
67. LADCO Ozone TSD—2015 O3 NAAQS Moderate Area Attainment Demonstration. *LADCO* <https://www.ladco.org/> (2022).
68. Grubert, E. & Hastings-Simon, S. Designing the mid-transition: a review of medium-term challenges for coordinated decarbonization in the United States. *WIREs Climate Change* **13**, e768 (2022).
69. The Emissions & Generation Resource Integrated Database. Technical Guide, eGrid2019. *EPA* https://www.epa.gov/sites/default/files/2021-02/documents/egrid2019_technical_guide.pdf (2021).
70. Jordahl, K. et al. GeoPandas Version 0.9.0. *Zenodo* <https://doi.org/10.5281/zenodo.4569086> (2021).
71. Manson, S., Schroeder, J., Van Riper, D., Kugler, T. & Ruggles, S. IPUMS National Historical Geographic Information System: Version 17.0 [5-Year Data [2015–2019, Block Groups & Larger Areas]]. *IPUMS* <https://doi.org/10.18128/D050.V17.0> (2022).
72. Raich, W., Fant, C., Jackson, M. & Roman, H. *Memorandum Supporting Near-Source Health Benefits Analyses Using Fine-Scale Incidence Rates* (Industrial Economics, Inc., 2020).
73. Turner, M. C. et al. Long-term ozone exposure and mortality in a large prospective study. *Am. J. Respir. Crit. Care Med* **193**, 1134–1142 (2016).
74. Emissions & Generation Resource Integrated Database (eGRID). *EPA* <https://www.epa.gov/egrid> (2022).
75. Cartographic boundary files. *US Census Bureau* <https://www.census.gov/geographies/mapping-files/time-series/geo/cartographic-boundary.html> (2022).
76. NERC regions. *EIA* <https://atlas.eia.gov/datasets/eia::nerc-regions/about> (2020).

Acknowledgements

Research reported in the publication was supported by US National Science Foundation awards CBET-1848683 and CAREER-CAS-Climate-2239834 to DEH, an Environmental Defense Fund (EDF) grant to D.E.H., a McCormick Center for Engineering Sustainability and Resilience seed grant to D.E.H., the Ubben Program for Carbon and Climate Science postdoctoral fellowship to J.L.S., The Data Science fellowship from the National Science Foundation Research Traineeship and Northwestern Integrated Data-Driven Discovery in Earth and Astrophysical Sciences to A.M., and an undergraduate research grant from Northwestern University to M.A.V. We thank W. Raich, H. Roman and M. Jackson from Industrial Economic and N. Fann, E. Chan and A. Kamal from the US EPA for deriving and providing the census tract-level all-cause mortality rates used in this study, as well as EDF experts for valuable equity framing feedback.

Author contributions

S.F.C., A.M., M.A.V., J.L.S., Z.E.A., M.J., E.A.G., S.C.A. and D.E.H. designed research, S.F.C., A.M. and M.A.V. performed research, S.F.C., A.M. and M.A.V. analysed data, S.F.C. wrote the original manuscript draft, and S.F.C., A.M., M.A.V., J.L.S., E.A.G., S.C.A. and D.E.H. provided edits.

Competing interests

The authors declare no competing interests.

Additional information

Supplementary information The online version contains supplementary material available at <https://doi.org/10.1038/s41893-023-01219-0>.

Correspondence and requests for materials should be addressed to Sara F. Camilleri.

Peer review information *Nature Sustainability* thanks Dena Montague and the other, anonymous, reviewer(s) for their contribution to the peer review of this work.

Reprints and permissions information is available at www.nature.com/reprints.

Publisher's note Springer Nature remains neutral with regard to jurisdictional claims in published maps and institutional affiliations.

Open Access This article is licensed under a Creative Commons Attribution 4.0 International License, which permits use, sharing, adaptation, distribution and reproduction in any medium or format, as long as you give appropriate credit to the original author(s) and the source, provide a link to the Creative Commons license, and indicate if changes were made. The images or other third party material in this article are included in the article's Creative Commons license, unless indicated otherwise in a credit line to the material. If material is not included in the article's Creative Commons license and your intended use is not permitted by statutory regulation or exceeds the permitted use, you will need to obtain permission directly from the copyright holder. To view a copy of this license, visit <http://creativecommons.org/licenses/by/4.0/>.

© The Author(s) 2023

Reporting Summary

Nature Portfolio wishes to improve the reproducibility of the work that we publish. This form provides structure for consistency and transparency in reporting. For further information on Nature Portfolio policies, see our [Editorial Policies](#) and the [Editorial Policy Checklist](#).

Statistics

For all statistical analyses, confirm that the following items are present in the figure legend, table legend, main text, or Methods section.

- | n/a | Confirmed |
|-------------------------------------|--|
| <input type="checkbox"/> | <input checked="" type="checkbox"/> The exact sample size (n) for each experimental group/condition, given as a discrete number and unit of measurement |
| <input checked="" type="checkbox"/> | <input type="checkbox"/> A statement on whether measurements were taken from distinct samples or whether the same sample was measured repeatedly |
| <input checked="" type="checkbox"/> | <input type="checkbox"/> The statistical test(s) used AND whether they are one- or two-sided
<i>Only common tests should be described solely by name; describe more complex techniques in the Methods section.</i> |
| <input checked="" type="checkbox"/> | <input type="checkbox"/> A description of all covariates tested |
| <input checked="" type="checkbox"/> | <input type="checkbox"/> A description of any assumptions or corrections, such as tests of normality and adjustment for multiple comparisons |
| <input type="checkbox"/> | <input checked="" type="checkbox"/> A full description of the statistical parameters including central tendency (e.g. means) or other basic estimates (e.g. regression coefficient) AND variation (e.g. standard deviation) or associated estimates of uncertainty (e.g. confidence intervals) |
| <input checked="" type="checkbox"/> | <input type="checkbox"/> For null hypothesis testing, the test statistic (e.g. F , t , r) with confidence intervals, effect sizes, degrees of freedom and P value noted
<i>Give P values as exact values whenever suitable.</i> |
| <input checked="" type="checkbox"/> | <input type="checkbox"/> For Bayesian analysis, information on the choice of priors and Markov chain Monte Carlo settings |
| <input checked="" type="checkbox"/> | <input type="checkbox"/> For hierarchical and complex designs, identification of the appropriate level for tests and full reporting of outcomes |
| <input type="checkbox"/> | <input checked="" type="checkbox"/> Estimates of effect sizes (e.g. Cohen's d , Pearson's r), indicating how they were calculated |

Our web collection on [statistics for biologists](#) contains articles on many of the points above.

Software and code

Policy information about [availability of computer code](#)

- | | |
|-----------------|---|
| Data collection | The WRF-CMAQ two-way model source code used for this numerical model study can be downloaded here (WRF: https://www2.mmm.ucar.edu/wrf/users/download/get_sources.html ; CMAQ: https://github.com/USEPA/CMAQ). Simulations were conducted using WRF-CMAQ v5.2 and WRF v3.8. The 2016 SMOKE Beta platform was used for allocating emissions to a 1.3km grid with county total emissions from the 2016v7.2 NEI and 1.3 km spatial surrogate provided by the Lake Michigan Air Directors Consortium (LADCO) and available on request. State boundaries are obtained using Cartopy v0.18.0 (https://doi.org/10.5281/zenodo.8216315) while Chicago shapefiles are available from the Chicago Data Portal via https://data.cityofchicago.org/ . All other related code used for our Vehicle-to-EGU Electricity Assignment and Emission Remapping Algorithm, health impacts and environmental justice implications can be found here: https://doi.org/10.5281/zenodo.8234544 |
| Data analysis | All analysis was conducted using: R Version 4.2.2, Python Version 3.8.12 with the GeoPandas package for determining census tract level air pollution concentrations Version 0.9.0 and Microsoft Excel Version 16.66.1. All scripts are available here (https://github.com/NU-CCRG/Camilleri-et-al-2022_WRF-CMAQ-eHDVstudy) |

For manuscripts utilizing custom algorithms or software that are central to the research but not yet described in published literature, software must be made available to editors and reviewers. We strongly encourage code deposition in a community repository (e.g. GitHub). See the Nature Portfolio [guidelines for submitting code & software](#) for further information.

Data

Policy information about [availability of data](#)

All manuscripts must include a [data availability statement](#). This statement should provide the following information, where applicable:

- Accession codes, unique identifiers, or web links for publicly available datasets
- A description of any restrictions on data availability
- For clinical datasets or third party data, please ensure that the statement adheres to our [policy](#)

As inputs to our Vehicle-to-EGU Electricity Assignment and Emission Remapping Algorithm we use: a grid gross loss across the U.S. from EPA (2021), the eGRID-2016 database for EGU details related to location, age and capacity with shapefiles from U.S. Census Cartographic boundary shapefiles and NERC. Model output is hosted on Northwestern's servers. Due to model output size limitation, specific model output requests can be made to the corresponding author. For our health and equity impacts, population and demographic data was obtained from the American Community Survey (ACS 2015-2019) and can be downloaded from here: <http://doi.org/10.18128/D050.V17.0>, baseline all-cause mortality incidence rates were obtained from Industrial Economic, Incorporated (IEc 2010-2015) and are available on request, β values were obtained from the Health Effects Institute report (HEI, 2022) for NO₂ and PM_{2.5} and from Turner et al. (2016) for O₃.

Human research participants

Policy information about [studies involving human research participants and Sex and Gender in Research](#).

Reporting on sex and gender	<input type="text" value="This is not a study involving human research participants"/>
Population characteristics	<input type="text" value="This is not a study involving human research participants"/>
Recruitment	<input type="text" value="This is not a study involving human research participants"/>
Ethics oversight	<input type="text" value="This is not a study involving human research participants"/>

Note that full information on the approval of the study protocol must also be provided in the manuscript.

Field-specific reporting

Please select the one below that is the best fit for your research. If you are not sure, read the appropriate sections before making your selection.

Life sciences Behavioural & social sciences Ecological, evolutionary & environmental sciences

For a reference copy of the document with all sections, see [nature.com/documents/nr-reporting-summary-flat.pdf](https://www.nature.com/documents/nr-reporting-summary-flat.pdf)

Ecological, evolutionary & environmental sciences study design

All studies must disclose on these points even when the disclosure is negative.

Study description	<input type="text" value="This is a numerical modeling study. All our analysis and findings are based on simulated data from sensitivity experiments."/>
Research sample	<input type="text" value="We conduct a total of 3 experiments:
(a) A baseline simulation (no vehicles are electric)
(b) Sensitivity experiment 1 - Electrifying 30% of heavy duty vehicles with not changes to the electric grid
(c) Sensitivity experiment 2 - Electrifying 30% of heavy duty vehicles assuming all additional energy demand is met by renewables"/>
Sampling strategy	<input type="text" value="Each experiment was run for a total of 4 months. Annual means presented in this study represent the average of the 4 simulated months."/>
Data collection	<input type="text" value="Model simulations were performed by Anastasia Montgomery and Sara F. Camilleri with output hosted on Northwestern's servers."/>
Timing and spatial scale	<input type="text" value="Each model simulation was run for a total of 4 months (Jul 2018, Oct 2018, Jan 2019 and April 2019) and focus our analysis to the region surrounding North America's largest freight hub, Chicago, Illinois. Simulations are conducted a spatial resolution of 1.3km."/>
Data exclusions	<input type="text" value="The first 10 days of each simulation was not included in the analysis to all for model spin up."/>
Reproducibility	<input type="text" value="All simulations are numerical modeling experiments"/>
Randomization	<input type="text" value="Temporal constraints"/>
Blinding	<input type="text" value="Blinding was not included as this is a numerical modeling study"/>

Did the study involve field work? Yes No

Reporting for specific materials, systems and methods

We require information from authors about some types of materials, experimental systems and methods used in many studies. Here, indicate whether each material, system or method listed is relevant to your study. If you are not sure if a list item applies to your research, read the appropriate section before selecting a response.

Materials & experimental systems

- | n/a | Involvement in the study |
|-------------------------------------|--|
| <input checked="" type="checkbox"/> | <input type="checkbox"/> Antibodies |
| <input checked="" type="checkbox"/> | <input type="checkbox"/> Eukaryotic cell lines |
| <input checked="" type="checkbox"/> | <input type="checkbox"/> Palaeontology and archaeology |
| <input checked="" type="checkbox"/> | <input type="checkbox"/> Animals and other organisms |
| <input checked="" type="checkbox"/> | <input type="checkbox"/> Clinical data |
| <input checked="" type="checkbox"/> | <input type="checkbox"/> Dual use research of concern |

Methods

- | n/a | Involvement in the study |
|-------------------------------------|---|
| <input checked="" type="checkbox"/> | <input type="checkbox"/> ChIP-seq |
| <input checked="" type="checkbox"/> | <input type="checkbox"/> Flow cytometry |
| <input checked="" type="checkbox"/> | <input type="checkbox"/> MRI-based neuroimaging |